Scientific Research Publishing

Advances in Nanoparticles, 2026, 15(3), 59-80
https://www.scirp.org/journal/anp
ISSN Online: 2169-0529
ISSN Print: 2169-0510

Biosynthesis of Silver Nanoparticles Using Pomegranate Peel Extract for Removal of Metal Ions

Hussein M. Ahmed[1*], Mohamed Nazih Abdallah[1], Lames A. Mohamed[1], Mohamed A. El-Khateeb[2]

[1]Sanitary and Environmental Engineering Institute, Housing and Building National Research Center (HBRC), Cairo, Egypt
[2]Water Pollution Research Department, National Research Center, Cairo, Egypt
Email: *Hussein_fee@yahoo.com, mohamed.nazih@dorsch.com, elkhateebcairo@yahoo.com, mohamed.alkhateeb@dorsch.com

How to cite this paper: Ahmed, H.M., Abdallah, M.N., Mohamed, L.A. and El-Khateeb, M.A. (2026) Biosynthesis of Silver Nanoparticles Using Pomegranate Peel Extract for Removal of Metal Ions. *Advances in Nanoparticles*, **15**, 59-80.
https://doi.org/10.4236/anp.2026.153003

Received: April 7, 2026
Accepted: August 25, 2026
Published: August 28, 2026

Abstract

This study explores the potential of biosynthesis technology in producing silver nanoparticles (AgNPs) using pomegranate peel extract as a reducing agent, and evaluation of their P-AgNPs for removing heavy metals such as lead (Pb), nickel (Ni), cadmium (Cd), and chromium (Cr), from aqueous solutions. The synthesis of P-AgNPs was confirmed by Fourier Transform Infrared Spectroscopy (FT-IR), X-ray Diffraction (XRD), Transmission Electron Microscopy (TEM), Energy Dispersive X-ray Spectroscopy (EDX), and Ultra-Violet Visible Spectroscopy (UV-Vis) analysis. The adsorption efficiency was influenced by factors such as metal ion concentration, contact time, pH levels, and the amount of adsorbent used. Functional groups played a significant role in enhancing metal ion reduction, as evidenced by the FT-IR spectrum peaks at 3400, 2900, 1600, 1550, and 1000 cm^{-1}, which contributed to the adsorption process. Additionally, the UV-Vis spectrum exhibited a resonance peak at 386 nm, indicating the successful interaction of bio-components from the PPE solution during nanoparticle synthesis. EDX analysis confirmed the elemental composition, with a strong peak corresponding to silver at 3.6 keV. The XRD analysis confirmed the crystalline phase of P-AgNPs in the synthesized nanoparticles. The data correlated with TEM findings, validating the nanoscale properties of the P-AgNPs. The adsorbent exhibited a maximum removal efficiency of Cr (11.00%), Pb (99.97%), Ni (87.60%), and Cd (99.10%) under optimum conditions of contact time (60 min), adsorbent dose (0.3 g/L), initial metal ion concentration of 1.0 mg/L, and pH (6.0). Equilibrium data were best fitted by the Freundlich isotherm (R^2 close to 0.987), indicating heterogeneous multilayer adsorption, the pseudo-first-order model was a better fit to the experimental data. This study highlights the potential application of biosynthe-

sized P-AgNPs in water purification by efficiently eliminating metal contaminants.

Keywords

Green Biosynthesis, Silver Nanoparticles, Pomegranate Peel, Metal Ions

1. Introduction

Pollution is a major source of many environmental problems, including water pollution, as water is an important component of life. Adhering to water quality regulations is essential to ensure the removal of hazardous chemicals from wastewater before its discharge into the environment [1] [2]. Heavy metal contamination remains a major global concern, making the treatment of industrial wastewater a critical environmental priority [3]-[5]. Heavy metals are poorly biodegradable and pose significant harmful effects on the environment [5] [6]. Certain heavy metals can bind to active enzyme sites in the body, leading to enzyme inhibition [1] [4]. Therefore, their removal from wastewater through various treatment techniques is essential [7]-[9]. This technology is highly effective and economical for treating aqueous effluents, offering advantages such as cost efficiency, ease of design and use, and minimal reliance on hazardous chemicals. Its superiority over methods like ion exchange and precipitation is attributed to the inherent beneficial properties of magnetic particles [10].

Nanoparticles typically range in size from 1 to 100 nm and possess a highly specific surface area [11]. Various physicochemical techniques are used to prepare and stabilize nanoparticles [10]-[15]. Silver nanoparticles can be synthesized using various methods, including laser ablation, photochemical synthesis, green biosynthesis, phase transfer techniques, and micro-emulsions. The green biosynthesis method is specifically used to obtain P-AgNPs, utilizing natural materials as reducing agents in the reduction process. Compared to chemical and physical methods, green synthesis is more environmentally friendly and yields a higher production of nanoparticles [15]. P-AgNPs that are extremely small have peculiar properties relative to bulk metals, which have piqued scientific curiosity and led to their usage as an anti-microbial agent [15] [16]. Nanoparticles are widely used in water treatment, textile engineering, and bioengineering [17].

Several studies have successfully synthesized silver nanoparticles using pomegranate peel extract, with reported applications in anti-microbial treatments, catalytic degradation of organic pollutants, antioxidant formulations, and the removal of heavy metals from wastewater. Green nanotechnology presents significant opportunities, particularly in waste recycling and the agricultural industry. Large quantities of leftover fruits and vegetables are discarded daily, yet these waste materials contain recyclable chemicals that can be repurposed to produce bioactive materials and new products. Plant extracts used in nanoparticle synthe-

sis often contain antioxidants such as flavonoids and phenolic acids, which possess beneficial functional groups. These functional groups play a key role in reducing metals into their corresponding metallic nanoparticles [18] [19]. Pomegranate peels are known to contain flavonoids, lignin, phenols, tannins, and cellulose, along with other bioactive compounds that offer various beneficial properties [19].

Pomegranate peel is rich in bioactive compounds such as flavonoids, lignin, phenols, tannins, and cellulose, which play crucial roles in the green synthesis of silver nanoparticles (AgNPs). Flavonoids act as potent reducing agents due to their hydroxyl groups, facilitating the conversion of Ag^{+} ions to metallic Ag^{0}. Phenolic compounds similarly contribute to the reduction process through electron donation, while also stabilizing the formed nanoparticles by binding to their surface. Tannins, as high-molecular-weight polyphenols, not only reduce silver ions but also provide strong capping and chelating effects, preventing nanoparticle aggregation. Lignin, a complex aromatic biopolymer, can function as both a mild reducing agent and a stabilizing matrix due to its phenolic and methoxy groups. Cellulose, while not a strong reducing agent, contributes to nanoparticle stabilization by providing a polysaccharide framework that limits particle growth and aggregation. Together, these naturally occurring compounds enable an eco-friendly synthesis route that avoids toxic chemical reductants and produces stable, well-dispersed AgNPs [20].

In this study, P-AgNPs were synthesized using green synthesis approaches, utilizing waste-derived extracts, specifically pomegranate peels, as reducing agents. These P-AgNPs were developed for the adsorption of metal ions from synthetic solutions containing Pb, Ni, Cd, and Cr. Several experimental variables were examined, including adsorbent dose (0.10, 0.15, 0.20, 0.25, and 0.30 g), contact time (10, 20, 30, 40, 50, and 60 min), and initial metal ion concentration (0.50, 1.0, 1.50, 2.0, and 2.50 mg/L). The study explores the feasibility of synthesizing silver nanoparticles for heavy metal removal from water. The originality of this research lies in its environmentally friendly synthesis method and its practical application in water treatment. Unlike conventional chemical synthesis techniques, this approach minimizes environmental impact by utilizing natural waste extracts as both reducing and stabilizing agents. Additionally, the study advances nanotechnology in environmental remediation by demonstrating the effectiveness of biologically synthesized P-AgNPs in metal adsorption. Utilization of pomegranate peel extract as a natural and sustainable resource for P-AgNPs synthesis. Use Fourier Transform Infrared Spectroscopy (FT-IR), X-ray Diffraction (XRD), Transmission Electron Microscopy (TEM), Energy Dispersive X-ray Spectroscopy (EDX), and Ultra-Violet Visible Spectroscopy (UV-Vis) analysis to confirm nanoparticle formation, size, and stability. Carry out many parameters to determine optimal conditions for metal ions removal. This research highlights the potential of green nanotechnology for wastewater treatment, offering a sustainable and effective solution for heavy metal contamination.

2. Materials and Methods

2.1. Preparation of Silver Nanoparticle (P-AgNPs)

Pomegranate peel was sourced from a local food market in Giza, Egypt. The outer surface of the fruit was cleaned and rinsed with tap water. To prepare the extract, 50 g of dried (105˚C/2h) pomegranate peel was boiled in water for approximately 30 min in an Erlenmeyer flask. The resulting extract was then stored in a refrigerator at 4˚C [15] [19]. To synthesize P-AgNPs, 10 mL of pomegranate peel extract (PPE) was added to a 0.01 M $AgNO_3$ solution. The mixture was stirred for 2 h at 70˚C to facilitate nanoparticle formation [13] [21] [22]. It has been reported that higher temperatures and concentrations can promote nanoparticle aggregation due to increased collision frequency among particles (Chekli *et al.*, 2013) [23]. As shown in **Figure 1**, the color changed from pale yellow to dark, confirming the synthesis of P-AgNPs [22]. This color transformation is attributed to the reducing agent present in the extract [1] [17] [24].

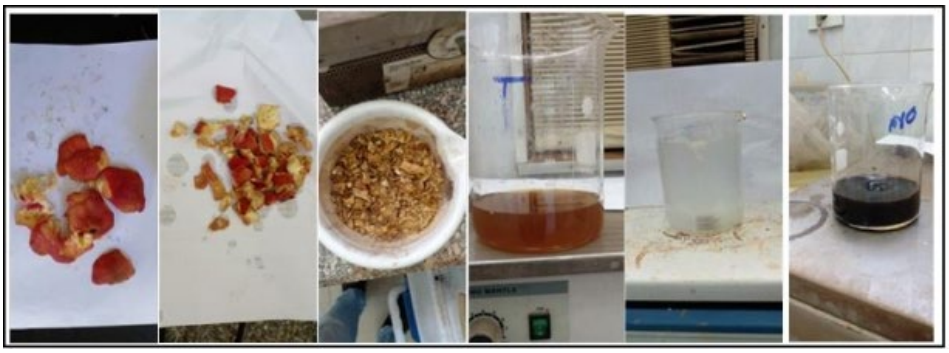

Figure 1. Steps of synthesis of P-Ag-NPs using pomegranate peel.

2.2. Batch Adsorption Studies

Analytical grade lead nitrate ($Pb(NO_3)_2$), Nickel nitrate ($Ni(NO_3)_2{\cdot}6H_2O$), cadmium nitrate tetrahydrate ($Cd(NO_3)_2{\cdot}4H_2O$), and chromium nitrate pentahydrate $Cr(NO_3)_3{\cdot}9H_2O$ were purchased from Sigma Aldrich (≥99% purity). Stock solutions (1000 mg/L) of each heavy metal were prepared using deionized water and subsequently diluted to the required concentrations. All experiments were conducted at (25 ± 3)˚C with a shaking speed of 150 rpm. In each test, the adsorbent was placed into 1.0 L Erlenmeyer flasks, the mixture was agitated using a Thermo Scientific shaker, after the reaction phase, the heavy metal ion content was determined using an atomic absorption spectrometer (Thermo Fisher Scientific ICE 3000 AAS). The adsorption of Cd, Ni, Cr, and Pb onto P-AgNPs was evaluated at different contact times (0, 10, 20, 30, 40, 50, and 60 min) at 1.0 mg/L and 0.20 g. The effect of adsorbent dose was also investigated by adding varying amounts of P-AgNPs (0.10, 0.15, 0.20, 0.25, and 0.30 g) at 60 min, its optimum contact time, and 1.0 mg/L [25]-[27]. To assess the influence of pH on adsorption processes, the adsorption of Cd, Ni, Cr, and Pb onto P-AgNPs was studied at different pH levels (1.0, 3.0, 5.0, and 8.0) at 0.30 g and 60 min [11]. The adsorption experiments

were performed using 100 mL working solution volume. The pH was adjusted using 0.1 M HCl and 0.1 M NaOH solutions. In addition, the synthesis procedure was revised to clearly indicate that 10 mL of pomegranate peel extract was mixed with 90 mL of 0.01 M $AgNO_3$ solution under continuous stirring at 70˚C for 2 h. The removal percentage (R%) was calculated using Equation (1) [27], where Ci and Ce represent concentrations at initial and equilibrium conditions, respectively.

$$\mathrm{R}\% = \frac{C_o - C_e}{C_o} \times 100 . \tag{1}$$

All adsorption experiments were conducted in triplicate (n = 3). The reported values represent mean ± standard deviation (SD). Statistical analysis was performed using Excel sheet, and differences were considered statistically significant at $p < 0.05$.

2.3. Adsorption Study

The amount of metal ions adsorbed onto the adsorbent was determined using Equation (2) [28] [29]. The adsorption equilibrium was analyzed using isotherm models, where the Langmuir isotherm model is represented by Equations (3) - (4), while the Freundlich isotherm model is described by Equation (5). Additionally, the adsorption kinetics of P-AgNPs were evaluated using Equations (6) - (7) [27] [30].

$$q_e\left(\mathrm{mg/g}\right) = \frac{\left(C_o - C_e\right)V}{m}, \tag{2}$$

$$\frac{C_e}{q_e} = \frac{1}{q_{\max}}, K_1 + \frac{C_e}{q_{\max}}, \tag{3}$$

$$R_L = \frac{1}{1 + C_o}, K_1, \tag{4}$$

$$\log q_e = \log K_f + \frac{1}{n}\log C_e, \tag{5}$$

$$\log\left(q_{eq} - q_t\right) = \log q_{eq} - k_1, t / 2.303, \tag{6}$$

$$\frac{t}{q_t} = \frac{1}{k_2 q_{eq}^2} + \frac{t}{q}, \tag{7}$$

where R% is the removal efficiency, q_e is the amount of pollutants adsorbed per unit mass of adsorbent (mg/g), C_0 is the initial concentration (mg/L), C_e is the concentration after adsorption (mg/L), m is the mass of the adsorbent (g), and V is the volume of the solution (L), $q_{\max}$ is the highest amount of pollutants needed to produce a monolayer (mg/g). The Langmuir constants are denoted by $q_{\max}$ and K_L. The linear plot of C_e/q_e vs C_e can be used to calculate the values of q_m and K_L, $1/n$ = Intensity parameter and K is the Freundlich equilibrium constant (mg/g). Freundlich approach is represented by the Equation, which plots $\log q_e$ vs. $\log C_e$ linearly. q_t is the amount adsorbed at time t mg/g^{-1} in t time (min), q_{eq} denotes the

amount adsorbed at equilibrium, mg/g^{-1} and k_1 is the pseudo-first-order constant (min^{-1}). Equation (7) and Equation (8) are not more than pseudo-first- and second-order adsorption kinetics. models. The q_{eq} and q_t are adsorption capacity at equilibrium and time, t, respectively. Also, K_1 and K_2 are pseudo-first and second-order kinetic constants, respectively.

3. Results and Discussion

3.1. Characterization of Synthesized P-AgNPs

UV-Vis spectroscopy is highly sensitive to the presence of silver nanoparticles (P-AgNPs). The maximum absorption band is observed at a wavelength of 386 nm, which is influenced by the size and shape of the nanoparticles. A UV-Vis absorption peak at 386 nm confirms successful AgNP synthesis because it matches the expected SPR signature of small, stable, and well-dispersed silver nanoparticles, indicating that metallic silver was formed and is present in the desired nanoscale state. As shown in Figure 2, the highest absorbance occurs at 386 nm in the UV-Vis spectrum. In the green synthesis process, Ag^+ ions are reduced to Ag^0 by electron-rich functional groups in pomegranate peel phytochemicals, particularly hydroxyl groups in phenols, flavonoids, and tannins. These compounds undergo oxidation to their corresponding oxidized derivatives while acting as both reducing and stabilizing agents for the silver nanoparticles, which, in turn, reduce Ag^+ ions to Ag^0. The mechanism of this reduction process is described by Equations (8) - (9).

$$AgNO_3 \rightarrow Ag^+ + NO_3^- . \tag{8}$$

$$e^- + Ag^+ \rightarrow Ag^0 . \tag{9}$$

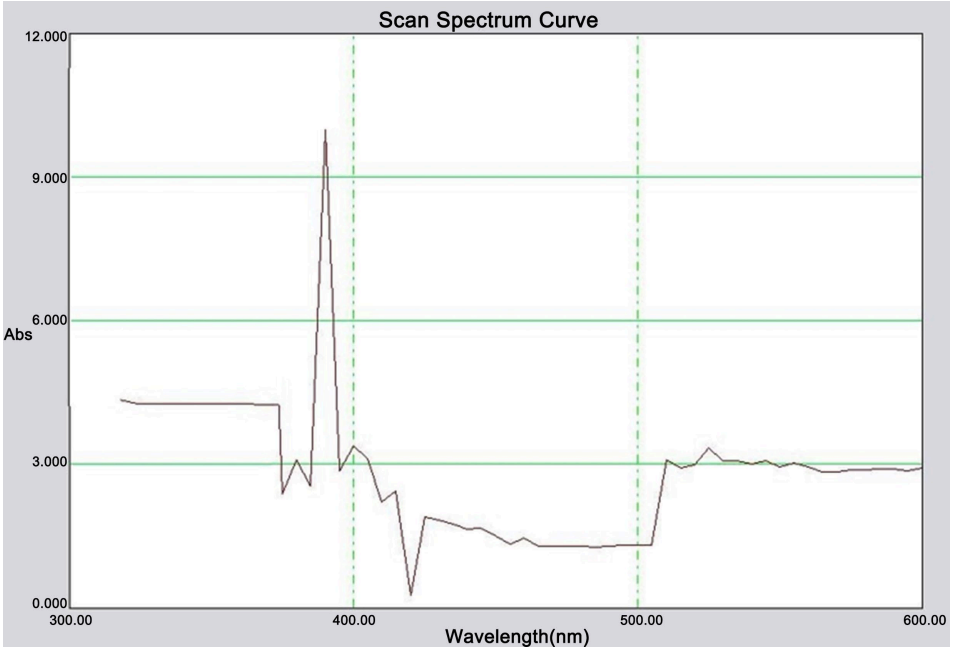

Figure 2. The UV-Vis spectrum of P-AgNPs.

The XRD pattern of the synthesized P-AgNPs displayed distinct diffraction peaks at $2\theta \approx 38.11^{\circ}$, 44.30°, 64.44°, and 77.3°. As shown in **Figure 3**, these peaks can be indexed to the (111), (200), (220), and (311) crystallographic planes of face-centered cubic (fcc) metallic silver, in accordance with the Joint Committee on Powder Diffraction Standards (JCPDS Card No. 04-0783). The (111) plane at ~38.1˚: This is typically the most intense peak for fcc silver and indicates a high degree of crystallinity. A dominant (111) reflection often suggests Preferential crystal growth along this plane, which can enhance certain physicochemical properties such as catalytic activity. The (200) reflection at ~44.3˚ and (220) at ~64.4˚. The (311) peak at ~77.3˚: This further supports the complete formation of the crystalline silver phase, with no detectable peaks from silver oxide or other impurities. The absence of additional diffraction peaks confirms that the synthesized product is phase-pure metallic silver, with no crystalline contaminants. The sharpness of the peaks, despite nanoscale size, indicates a relatively high degree of crystallinity [9]. The XRD results clearly show that the Ag nanoparticles synthesized by the extract are crystalline in nature. The XRD results clearly show that the Ag nanoparticles synthesized by the extract are crystalline in nature.

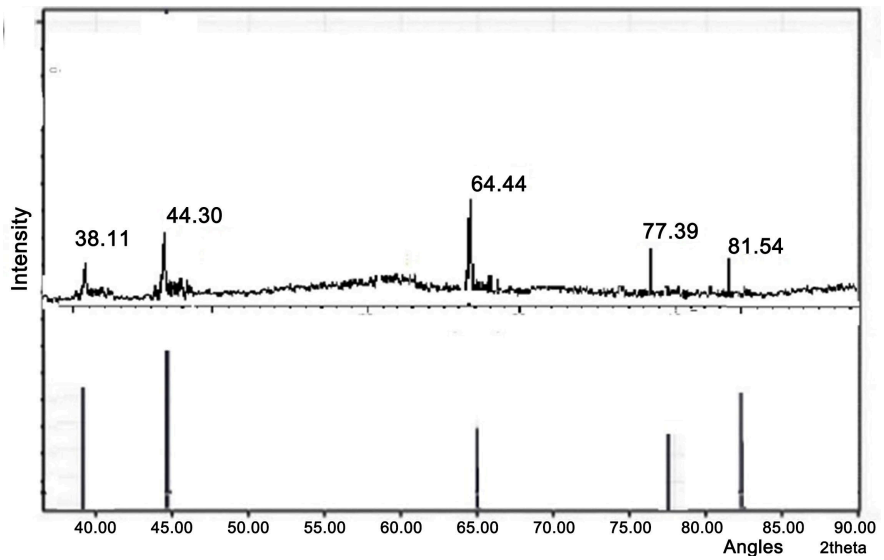

Figure 3. The X-ray Diffraction (XRD) spectra of the prepared P-AgNPs nanoparticles.

The FT-IR spectra were used to identify the characteristic peaks of P-AgNPs, highlighting the role of biomolecules in pomegranate extracts in reducing silver ions to silver nanoparticles. **Figure 4** presents the FT-IR spectra of P-AgNPs, confirming the presence of functional groups involved in the synthesis process. The broad band at 3406 cm^{-1} corresponds to the O-H stretching vibration of hydrogen-bonded alcohols and phenols. The absorbance peak at 2900 cm^{-1} indicates the presence of C-H stretching in alkenes. The band observed near 1600 cm^{-1} is more consistent with C=C stretching (aromatic ring vibrations) or a conjugated C=O (carbonyl/amide I) mode rather than C-O or alkynic vibrations. C-O stretching

vibrations typically appear in the 1000 - 1300 cm^{-1} region, while alkyne (C≡C) stretches are expected around 2100 - 2260 cm^{-1} and are often weak. C-N stretching modes occur broadly between ~1020 and 1360 cm^{-1} and may overlap with C-O bands. Additionally, a sharp peak attributed to the C=O stretching vibration appears, followed by another peak at 1018 cm^{-1}. These functional groups confirm the successful synthesis and stabilization of P-AgNPs [31] [32].

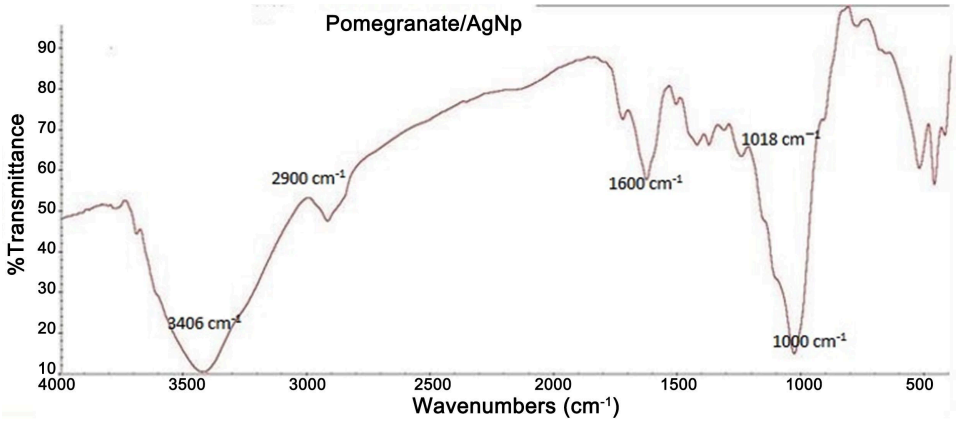

Figure 4. FT-IR spectrum of P-AgNPs.

To confirm that the silver particles are indeed in the nanoscale range, additional characterization using Transmission Electron Microscopy (TEM) is required. TEM offers high-resolution imaging that can directly visualize individual nanoparticles, allowing accurate determination of particle size distribution, shape, and degree of aggregation, thereby validating their nanoscale dimensions. As shown in **Figure 5**, TEM analysis revealed that the synthesized silver nanoparticles were predominantly spherical with a relatively narrow size distribution, ranging from (10 - 50) nm. The images showed well-dispersed particles with minimal aggregation, indicating effective stabilization by the phytochemical capping agents derived from pomegranate peel extract. The nanoscale dimensions observed are consistent with the surface plasmon resonance (SPR) peak at 386 nm in the UV-Vis spectrum and with the crystallite size estimated from XRD via the Debye-Scherrer equation. The clear, sharp particle boundaries in TEM micrographs further confirm the high crystallinity of the P-AgNPs, supporting the XRD findings of an fcc silver lattice. Occasional slight clustering of nanoparticles may be attributed to drying effects during TEM grid preparation rather than actual solution-phase aggregation. Overall, the TEM results validate the successful synthesis of small, stable, and well-dispersed P-AgNPs suitable for high-efficiency adsorption applications.

The EDX analysis confirmed the elemental composition of the P-AgNPs, revealing a strong peak at 3.6 keV, corresponding to silver (53%). The EDX spectrum of the synthesized Ag nanoparticles is presented in **Figure 6**. The presence of the Ag signal in the EDX spectrum confirms the successful synthesis of silver nanoparticles. The measured atomic ratio of C/Ag = 20.5/13.6 reflects the relative

abundance of carbon (originating from the pomegranate peel phytochemicals used as reducing and capping agents) to metallic silver in the sample. The relatively high carbon content indicates that the AgNPs are coated with an organic layer rich in carbon-based functional groups (phenolic, hydroxyl, and carboxyl groups), which stabilize the nanoparticles, prevent aggregation, and may also contribute to their adsorption performance. These results validate the successful synthesis of P-AgNPs and the involvement of organic components from pomegranate extract in the nanoparticle formation [32] [33].

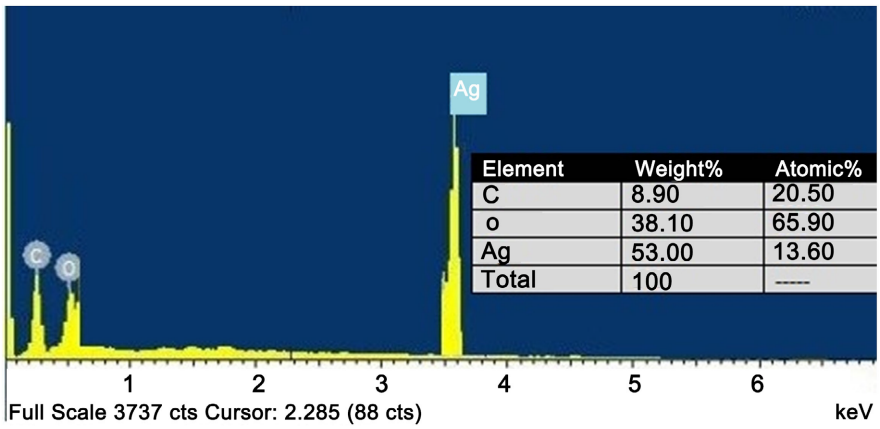

Figure 5. EDX analysis of P-AgNPs.

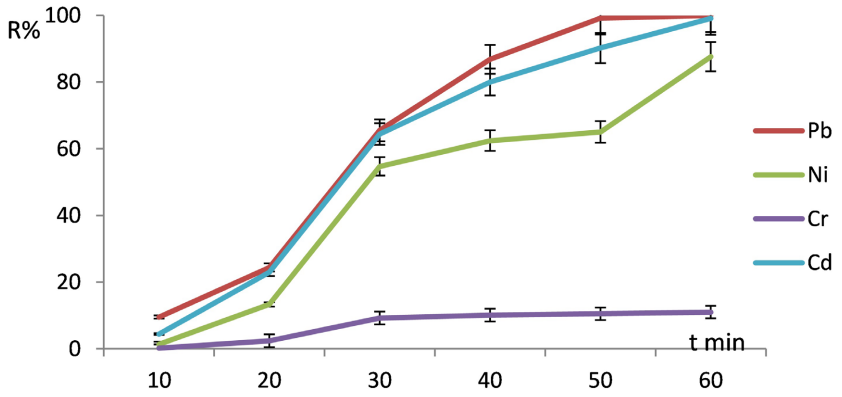

Figure 6. The EDX analysis of P-AgNPs.

3.2. Adsorption Saturation of P-AgNPs

The removal efficiency of Pb, Ni, Cd, and Cr at different adsorption times (10, 20, 30, 40, 50, and 60 min) was observed to be 99.97%, 87.60%, 99.10%, and 11.00%, respectively. The highest removal efficiency (R%) was obtained at the optimal adsorption time of 60 min, as illustrated in Figure 7.

These results are consistent with findings from previous studies (Ahmed *et al.*, 2023) [4], further validating the effectiveness of P-AgNPs in heavy metal adsorption.

The variation in removal efficiencies of P-AgNPs for Cr, Cd, Pb, and Ni can be

attributed to the differences in their physicochemical properties, particularly ionic radius, hydration energy, and charge. Metals with a larger ionic radius and lower hydration energy, such as Pb^{2+} (ionic radius ≈ 1.19 Å), generally exhibit stronger adsorption due to easier dehydration and more effective interaction with active sites on the nanoparticle surface. In contrast, smaller ions with higher hydration energy, such as Ni^{2+} (ionic radius ≈ 0.69 Å), require more energy to shed their hydration shell, reducing their affinity for the adsorbent. Cr^{3+}, having a higher charge (+3) and smaller radius (≈0.62 Å), tends to form strong electrostatic interactions, but its high hydration energy can limit adsorption unless surface sites are well-suited for trivalent ions. Cd^{2+}, with an intermediate ionic radius (≈0.95 Å) and moderate hydration energy, showed removal efficiencies between those of Pb^{2+} and Ni^{2+} (Table 1). Therefore, the observed adsorption trend aligns with the interplay between ion size, charge density, and hydration energy, which governs the strength of metal-adsorbent interactions.

Table 1. The physicochemical properties of metal ions.

Metal	Charge	Ionic radius
Pb^{2+}	+2	1.19 Å
Ni^{2+}	+2	0.69 Å
Cr^{3+}	+3	0.62 Å
Cd	+2	0.95 Å

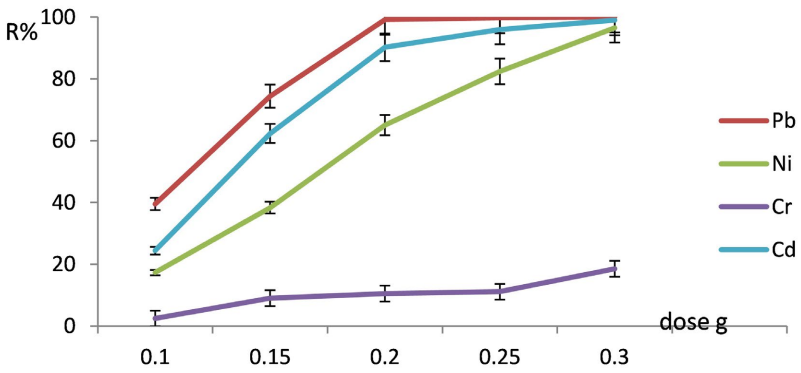

Figure 7. The removal efficiency of P-AgNPs for Cr, Cd, Pb, and Ni at different contact times.

The removal efficiencies of P-AgNPs at different adsorbent doses (0.10, 0.15, 0.20, 0.25, and 0.30 g/L) for Pb, Cd, Ni, and Cr were 100%, 99.02%, 96.50%, and 18.50%, respectively, as illustrated in Figure 8. The results indicate that the optimum P-AgNPs dose was 0.30 g/L. The increase in removal efficiency (R%) with higher adsorbent doses can be attributed to the availability of more vacant adsorption sites and free electrons, which enhance the degradation process. These findings align with previous studies (Sadon *et al.*, 2012) [27], further supporting the effectiveness of P-AgNPs in heavy metal adsorption.

The observed increase in removal efficiency with higher adsorbent doses is attributed to the greater number of available active sites on the P-Ag-NP surface, which enhances the probability of metal ions interacting with and binding to these sites. At lower doses, many target ions remain unbound due to insufficient active site availability, resulting in lower removal efficiency. As the adsorbent dose increases, more ions are captured, and efficiency rises until a saturation point is reached. Beyond this optimal dose, further increases in adsorbent amount do not yield significant improvements because most of the available metal ions in solution have already been adsorbed. At this stage, active sites remain unoccupied simply due to the lack of remaining ions, and particle-particle aggregation at high doses may further reduce the effective surface area.

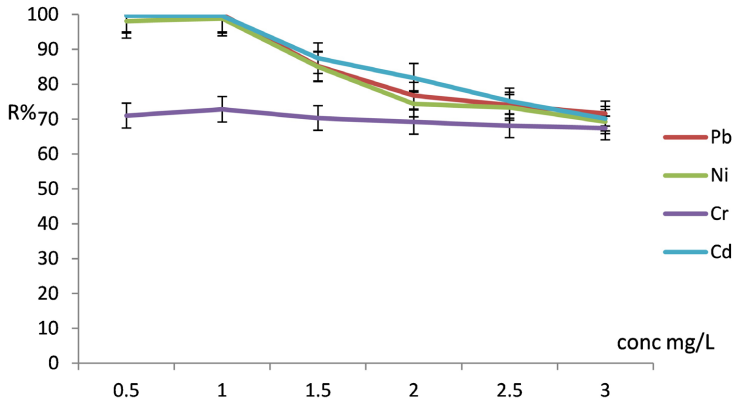

Figure 8. The removal efficiency of P-AgNPs for Cr, Cd, Pb, and Ni at different doses.

The adsorption efficiencies of Cr, Cd, Pb, and Ni at concentrations of 0.50, 1.0, 1.5, 2.0, and 2.5 mg/L using P-AgNPs were 100%, 99.99%, 99.67%, and 73.36%, respectively, as shown in **Figure 9**. These results highlight the exceptional capability of P-AgNPs for heavy metal removal, with Cr, Cd, and Pb achieving near-complete adsorption across all tested concentrations. The comparatively lower efficiency observed for Ni may be attributed to its smaller ionic radius and higher hydration energy, which limit its interaction with active sites on the nanoparticle surface.

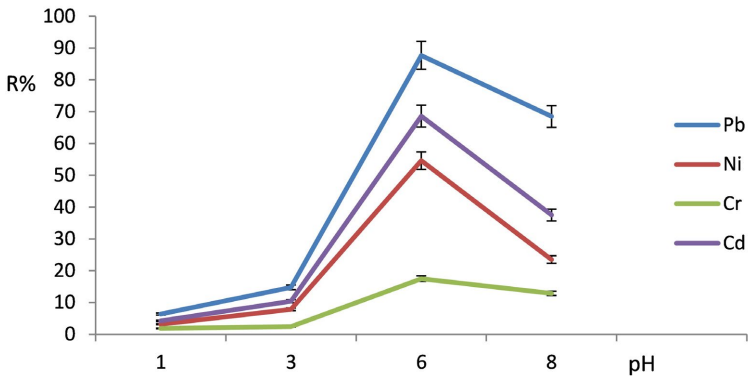

Figure 9. The removal efficiency of P-AgNPs for Cr, Cd, Pb, and Ni at different concentrations.

The pH of the solution plays a critical role in the adsorption process because it influences both the surface charge of P-AgNPs and the speciation of metal ions in solution. At low pH values, the surface of P-AgNPs tends to be protonated, resulting in a net positive charge. This causes electrostatic repulsion between the adsorbent and positively charged metal ions (Cr^{3+}, Cd^{2+}, Pb^{2+}, Ni^{2+}), reducing adsorption efficiency. In addition, excess H^+ ions compete with metal cations for active binding sites, further inhibiting metal uptake.

As pH increases toward a neutral or slightly alkaline range, deprotonation of functional groups (such as hydroxyl, carbonyl, and phenolic groups from the pomegranate peel phytochemicals coating the P-AgNPs) occurs, imparting a negative surface charge. This promotes electrostatic attraction between the negatively charged nanoparticle surface and the positively charged metal ions, enhancing adsorption efficiency. However, at excessively high pH values, some metal ions may precipitate as metal hydroxides rather than being adsorbed, complicating the adsorption mechanism. The interaction between P-AgNPs and metal ions during adsorption involves a combination of electrostatic attraction, surface complexation, and van der Waals forces. The phytochemical coating from pomegranate peel provides abundant electron-donating groups (-OH, -COOH, -C=O) that can chelate or coordinate with metal ions, while the nanoscale size of P-AgNPs offers a high surface area for binding. In some cases, weak physisorption may dominate, as indicated by pseudo-first-order kinetics, suggesting that the process is primarily governed by physical interactions rather than strong covalent bonding [28].

The highest removal efficiencies at an optimum pH of 6.0 were observed as follows: Cr (11.00%), Pb (99.97%), Ni (87.60%), and Cd (99.10%) as illustrated in Figure 10. The enhanced adsorption at pH 6.0 can be attributed to the increased availability of vacant sites for metal ion bio-sorption in an acidic medium. Additionally, the presence of negatively charged functional groups on the bio-sorbent surface at this pH facilitates stronger binding interactions with metal ions such as Cu, Pb, Se, Zn, and Cr, further enhancing adsorption performance [34]-[36].

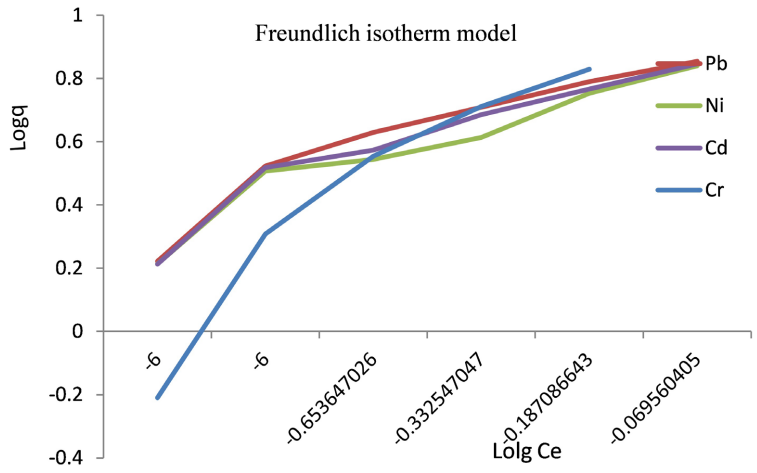

Figure 10. The removal efficiency of P-AgNPs for Cr, Cd, Pb, and Ni at different pH values.

3.3. Isotherm and Kinetic Study

The adsorption study of metal ions onto P-AgNPs was conducted under optimum operating conditions: an adsorbent dose of 0.30 g, a contact time of 50 min, and a pH of 6.0. Figure 11 and Table 2 present the Langmuir and Freundlich isotherm model values obtained from the study. The adsorption data for Cr, Cd, Pb, and Ni showed a better fit to the Freundlich isotherm model than to the Langmuir model, as indicated by the relatively higher correlation coefficient (R^2) values, which ranged from 0.8995 to 0.9256.

In adsorption studies, R^2 values closer to 1 indicate a stronger fit of the experimental data to the model, suggesting that the Freundlich equation adequately describes the adsorption behavior of the system. The superior fit to the Freundlich model implies that the adsorption occurs on a heterogeneous surface with sites of varying affinities, rather than on a uniform monolayer as assumed in the Langmuir model. This finding is consistent with the surface chemistry of P-AgNPs, where variations in surface functional groups, particle size, and morphology create a distribution of binding energies. In Table 2, the KF (Adsorption Capacity) = 694, a higher KF value indicates greater adsorption capacity, meaning P-AgNPs can remove a significant amount of metal ions from the solution. State that 1/n is approximately 0.25, and that this value indicates favorable adsorption on P-AgNPs, reflecting the nanoparticles' heterogeneous nature.

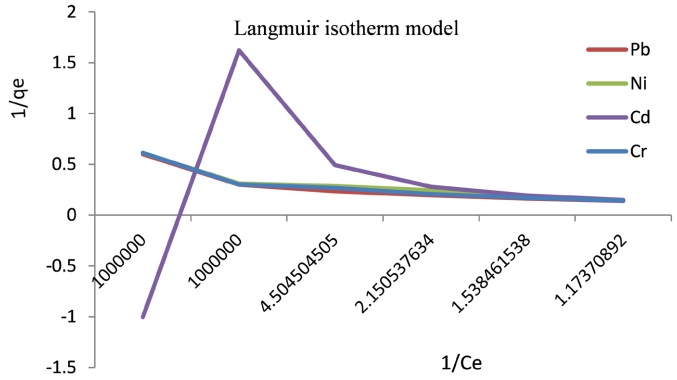

Figure 11. The Langmuir and Freundlich isotherm models of P-AgNPs.

Table 2. Correlation coefficients (R^2) of Langmuir and Freundlich models for the adsorption of metal ions into P-Ag-NPs.

Metal ions	Freundlich isotherm models	Langmuir isotherm models
Pb	0.8995	0.7134
Ni	0.9256	0.7435
Cd	0.9142	0.7112
Cr	0.9083	0.7636
K	694	0.267
q_{max}	506	90.9
n	4.15	-

Figure 12 and Table 3 compare the linear fits of the pseudo-first-order and pseudo-second-order kinetic models for the adsorption of Cr, Cd, Pb, and Ni onto P-AgNPs. The correlation coefficients (R^2) obtained for the pseudo-first-order model were consistently higher than those for the pseudo-second-order model, indicating a better fit to the experimental data. This suggests that the adsorption process is primarily governed by a physical adsorption (physisorption) mechanism, where metal ions are retained on the nanoparticle surface through weak van der Waals forces and electrostatic interactions rather than through chemisorption involving strong covalent or ionic bonds [36].

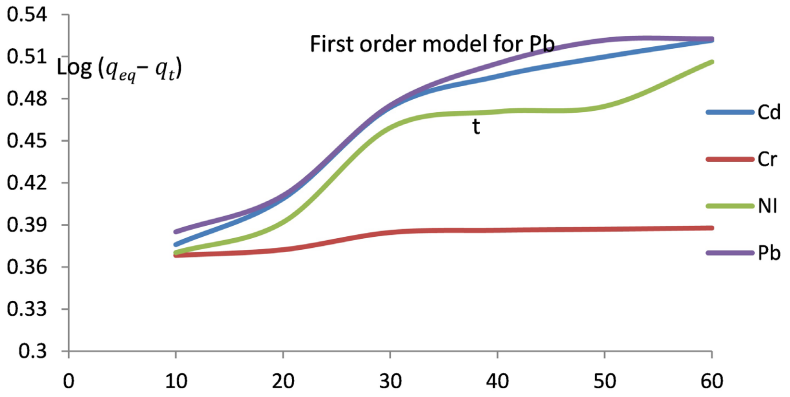

Figure 12. The first and second kinetic models of Cd, Pb, Ni and Cr ions onto P-AgNPs.

Table 3. Correlation coefficients (R^2) of the first and second kinetic models.

Process	Water consumption (m^3)	Electricity consumption (kWh)
Water	0.1	-
Drying	0	2.50
Crushing	0	1.0
$AgNO_3$ 1.0 kg	0	0
Total Consumption	0.10	3.5
Cost	1.0	10.50

3.4. Regeneration Study

The regeneration and reusability of P-AgNPs were evaluated under the optimum adsorption conditions. Desorption of the adsorbed metal ions was carried out using 0.1 M HCl as the regenerating agent. After each adsorption-desorption cycle, the recovered adsorbent was thoroughly washed with deionized water, dried, and reused in subsequent adsorption experiments. The regeneration efficiency was assessed by comparing the adsorption capacity of the regenerated adsorbent with its initial adsorption capacity.

The results demonstrated a progressive decline in adsorption performance with repeated regeneration cycles. The regeneration results demonstrated a gradual decline in the removal efficiency of the biosynthesized AgNPs adsorbent over suc-

cessive adsorption-desorption cycles. The removal efficiency decreased from approximately 95% in the first cycle to 83%, 54%, 39%, and finally 12% after the fifth cycle. This reduction in adsorption performance can be attributed to the progressive loss of active adsorption sites, partial structural deterioration of the adsorbent surface, and incomplete desorption of metal ions during the regeneration process. Furthermore, repeated exposure to adsorption and desorption conditions may lead to aggregation of silver nanoparticles and blockage of available binding sites, thereby reducing the adsorption capacity.

Despite the observed decline, the adsorbent maintained reasonable removal efficiency during the initial regeneration cycles, indicating its potential for reuse in wastewater treatment applications. However, the significant reduction in performance after multiple cycles suggests that further optimization of the regeneration procedure is required to improve the long-term stability and reusability of the adsorbent [37]-[40].

3.5. Reason for Increased Removal Efficiency in Early Cycles

In adsorption studies, removal efficiency improves slightly during the first few regeneration cycles. This can be attributed to regeneration. Can clean the surface, remove weakly bound impurities, and expose additional active sites that were initially blocked. The regeneration agent may also enhance surface charge characteristics (protonation, deprotonation), improving the affinity toward target pollutants. Repeated contact with aqueous media can increase surface hydrophilicity, swelling, or pore accessibility, making adsorbate diffusion into active sites easier. Some functional groups become more reactive or better oriented. After initial adsorption-desorption cycles, strengthening interactions with pollutants. The increase in removal efficiency during early regeneration cycles is most likely due to surface conditioning, where repeated regeneration enhances accessibility and reactivity of adsorption sites before efficiency stabilizes. or declines with prolonged use.

3.6. Cost of Adsorbents

The cost study of using P-AgNPs as adsorbents for removal of metal ions from an aqueous solution was calculated. The cost study for using P-AgNPs as adsorbents in metal ion removal from aqueous solutions was calculated and is presented in Table 4. The results indicate that the specific energy consumption for adsorbent production is 3.50 kWh/m^3 with water consumption = 0.10 m^3. The total cost required to produce 0.30 kg of the adsorbent is 11.50 Egyptian Pounds, equivalent to $0.23. This cost is significantly lower compared to other adsorbents, such as activated carbon (Ahmed *et al.* 2023) [4], and the adsorption process is environmentally friendly and does not generate secondary by-products. The cost-effectiveness of P-AgNPs as an adsorbent was evaluated by comparing both adsorption capacity and actual material cost with those of commonly reported adsorbents such as activated carbon, zeolite, and synthetic polymer-based resins. P-AgNPs exhibited

an adsorption capacity of [506 mg/g for metal ions], which is higher than the reported values for activated carbon (50 - 90) mg/g (Mohammadi *et al.*, 2010) [41] and natural zeolite (20 - 60) mg/g (Velarde *et al.*, 2024) [42]. The production cost of P-AgNPs was estimated at $0.23 per 0.3 kg, primarily due to the use of pomegranate peel, an agricultural waste product, as the reducing and stabilizing agent. In contrast, the cost of commercial activated carbon ranges from $0.83 and that of ion-exchange Resins from $0.94. These results indicate that P-AgNPs combine high adsorption efficiency with low raw material costs, making them a competitive and sustainable alternative for heavy metal removal.

Table 4. The energy and material consumption for production of 0.30 kg of P-AgNPs.

Process	Water consumption* (m^3)	Electricity consumption* (kWh)
Water	0.1	-
Drying	0	2.50
Crushing	0	1.0
$AgNO_3$ 1.0 kg	0	0
Total Consumption	0.10	3.5
Cost	1.0	10.50

*In Egypt, the cost of 1 m^3 of water for industrial use = 10.0 L.E.; *In Egypt, the cost of 1 kWh of electricity for industrial use = 3.0 L.E.

3.7. Comparison Study of P-AgNPs with Other Adsorbents for Heavy Metal Removal

The q_{max} values are reported from the cited literature (Langmuir q_{max} unless otherwise stated). Conditions (pH, T) (Qiaoqiao Su *et al.*, 2021) [43] aim to close the gap between high-capacity but slow microporous ion-exchangers and fast, high-surface-area materials (CF/GO). MOFs and some carbon materials may show decreased stability or require harsh and important operational considerations. Advanced materials (MOFs, GO, tuned ACFs) can be costly but useful for high-value or small-volume treatments (Table 5).

3.8. Future Scaling up of Green Method

In future work, we will validate the material under real wastewater conditions using grab and composite Influent/effluent samples from municipal and industrial sources and evaluation of regeneration/reuse over multiple cycles with mass balance of target pollutants. Analytical endpoints will include removal efficiency (COD/BOD, metals, dyes, pathogens as relevant), kinetics/isotherms in complex matrices. From these results, this study will guide process optimization and inform deployment pathways.

3.9. Potential for Scaling up of Green Method Synthesis

Uses non-toxic, renewable, and biodegradable materials (plant extracts, microbes,

agricultural waste), making it suitable for large-scale sustainable production. Often relies on inexpensive natural precursors and mild reaction conditions (ambient temperature, aqueous medium), reducing operational costs compared to conventional chemical synthesis. The absence of harsh chemicals and high-energy requirements allows scaling up with lower environmental and energy footprints. Green synthesis can be adapted into existing bioreactors or batch/continuous-flow systems, which makes integration into industrial production feasible. Growing demand for environmentally friendly nanomaterials/adsorbents (in water treatment, catalysis, biomedicine) supports the scalability and commercialization of the method.

Table 5. Comparison study of P-AgNPs with other adsorbents for heavy-metal removal.

Adsorbent (typical form)	Representative q_{max} (mg·g^{-1}) $Pb^{2+}/Cu^{2+}/Cd^{2+}/Ni^{2+}/Zn^{2+}$	Typical conditions reported	Key advantages	Limitations/remarks	Ref.
NaA Z	Pb: variable reports from tens to several hundred mg·g^{-1} (depends on synthesis/form); Cu: up to hundreds mg·g^{-1} reported (some extreme values ~700 - 800 mg·g^{-1} in specific studies).	Many studies pH 4 - 6, 20˚C - 25˚C; synthesis-dependent.	Excellent ion-exchange; widely used; can be synthesized from waste streams.	Wide spread in reported q_{max} depends strongly on preparation, particle size, pretreatment. See examples.	[43]
Activated carbon/activated carbon fibers (AC/ACF)	Pb: commonly 50 - 300 mg·g^{-1} (higher for functionalized ACFs; reports up to ~700 mg·g^{-1} for specialized fibers). Cu: often 20 - 200 mg·g^{-1}.	pH 4 - 6, 20˚C - 25˚C; depends on activation & functionalization.	Very high surface area, tunable surface chemistry, commercial availability; high q when functionalized.	Cost (high-grade ACF), regeneration can be energy-intensive; nonselective; performance varies greatly by activation/functional groups.	[44]
Graphene oxide/reduced GO (GO/rGO, composites)	Pb: commonly 100 - 300 mg·g^{-1} (examples: ~90 - 250 mg·g^{-1}), some functionalized GO reports > 200 mg·g^{-1}. Cu/Cd similar ranges.	pH 4 - 6, 20˚C - 25˚C; functionalization increases capacity.	Very high capacities, fast kinetics, rich surface chemistry for modification.	Cost, aggregation, recovery from water (magnetic composites help), possible toxicity concerns.	[45]
Chitosan/chitosan-based composites	Pb: wide range tens to several hundred mg·g^{-1} (some tailored chitosan composites report >200 - 700 mg·g^{-1} under specific conditions). Cu/Cd also high in modified chitosan.	Often best in acidic to near-neutral pH (pH 4 - 6).	Biopolymer (renewable), good affinity for metal cations, easy to functionalize/crosslink.	Mechanical strength, swelling, solubility in acid, and regeneration limitations unless crosslinked/composited.	[46]
Biochar/magnetic biochar	Pb: often 10 - 100 mg·g^{-1} (typical), optimized biochars may reach > 100 mg·g^{-1}; Cd/Zn somewhat lower.	pH 4 - 7, 20˚C - 30˚C.	Low-cost, waste-derived, facile production, good for large-scale low-cost remediation.	Lower capacity/selectivity vs advanced adsorbents; variability by feedstock/pyrolysis conditions.	[47]
Natural zeolite (clinoptilolite)	Pb: ~10 - 60 mg·g^{-1} typical; some thermal/chemical modifications increase capacity. Cu/Ni/Zn generally lower.	pH 4 - 7, 20˚C - 25˚C.	Cheap, abundant, decent ion-exchange; robust in columns.	Lower capacity than engineered materials; selectivity influenced by competing cations.	[48]

3.10. Limitations of Green Method Synthesis

Plant extracts or microbial cultures may vary seasonally and geographically, leading to inconsistencies in nanoparticle size, shape, and yield. Lack of precise control over reaction parameters (pH, temperature, concentration of bioactive compounds)

makes reproducibility difficult at an industrial scale. Removal of unreacted biomolecules or impurities can be difficult, time-consuming, and costly during scale-up. Some green methods produce lower yields compared to conventional chemical or physical synthesis routes.

Nanoparticles or bio-products synthesized by green methods may agglomerate or lose activity during storage, requiring stabilizers. Large-scale use of plant/microbial materials and their metabolites may face 448 regulatory hurdles (biosafety, quality control, toxicity testing).

4. Conclusion

In this study, P-AgNPs were successfully synthesized using a green synthesis method, where silver nitrate ($AgNO_3$) and pomegranate peel extract were utilized for the reduction of silver salt. The synthesized P-AgNPs were characterized using UV-Vis spectrophotometry, FT-IR, XRD, TEM and EDX. This study successfully synthesized pomegranate peel-mediated silver nanoparticles (P-AgNPs) and demonstrated their high efficiency in removing heavy metals (Cr, Cd, Pb, and Ni) from aqueous solutions. Characterization via UV-Vis spectroscopy, XRD, and kinetic/isotherm modeling confirmed the formation of small, crystalline, and well-dispersed nanoparticles with a heterogeneous adsorption surface. The maximum removal efficiencies were achieved under optimal conditions, with adsorption trends influenced by the ionic radius, charge, and hydration energy of the metals. The adsorbent exhibited a maximum removal efficiency of Cr (11.00%), Pb (99.97%), Ni (87.60%), and Cd (99.10%) under optimum conditions of contact time (60 min), adsorbent dose (0.3 g/L), initial metal ion concentration of 1.0 mg/L, and pH (6.0). Equilibrium data were best fitted by the Freundlich isotherm (R^2 close to 0.987), indicating heterogeneous multilayer adsorption. The pseudo-first-order model was a better fit to the experimental data. Compared to conventional chemical precipitation, ion exchange, or activated carbon adsorption, P-AgNPs offer a greener, low-cost, and efficient alternative that uses agricultural waste as a reducing agent, reduces secondary pollution, and operates effectively at low adsorbent dosages. These advantages make P-AgNPs a promising candidate for practical water purification applications, particularly in rural and resource-limited settings. In this work, the focus is evaluating reusability over five treatment cycles. Importantly, the material exhibited excellent regeneration performance, maintaining high removal efficiency across multiple cycles, which underscores its reusability and cost-effectiveness. Compared to conventional adsorbents such as activated carbon, graphene oxide, chitosan composites, bio-char, and natural zeolite, combined with its green synthesis approach and scalability, this makes the material highly promising for real-world wastewater treatment applications targeting toxic heavy metals.

Author Contributions

Conceptualization, Lames A. Mohamed; methodology, Hussein M. Ahmed; soft-

ware, Mohamed A. El-Khateeb; validation, Mohamed Nazih Abdallah; formal analysis, Hussein M. Ahmed; investigation, Hussein M. Ahmed; resources, Hussein M. Ahmed; data curation, Lames A. Mohamed; writing—original draft preparation, Hussein M. Ahmed; writing—review and editing, Hussein M. Ahmed; visualization, Lames A. Mohamed; supervision, Mohamed A. El-Khateeb; project administration, Mohamed Nazih Abdallah; funding acquisition, Hussein M. Ahmed. All authors have read and agreed to the published version of the manuscript.

Conflicts of Interest

The authors declare no conflicts of interest regarding the publication of this paper.

References

[1] Ahmed, H., El-Khateeb, M. and Ahmed, N. (2022) Effective Granular Activated Carbon for Greywater Treatment Prepared from Corncobs. *Egyptian Journal of Chemistry*, **65**, 255-263. https://doi.org/10.21608/ejchem.2022.117621.5302

[2] Geise, G.M., Lee, H., Miller, D.J., Freeman, B.D., McGrath, J.E. and Paul, D.R. (2010) Water Purification by Membranes: The Role of Polymer Science. *Journal of Polymer Science Part B: Polymer Physics*, **48**, 1685-1718. https://doi.org/10.1002/polb.22037

[3] Abdel Salam, O.E., Reiad, N.A. and ElShafei, M.M. (2011) A Study of the Removal Characteristics of Heavy Metals from Wastewater by Low-Cost Adsorbents. *Journal of Advanced Research*, **2**, 297-303. https://doi.org/10.1016/j.jare.2011.01.008

[4] Ahmed, H.M., Sobhy, N.A., Hefny, M.M., Abdel-Haleem, F.M. and El-Khateeb, M.A. (2023) Evaluation of Agrowaste Species for Removal of Heavy Metals from Synthetic Wastewater. *Journal of Environmental and Public Health*, **2023**, Article ID: 7419015. https://doi.org/10.1155/2023/7419015

[5] Nandal, M., Hooda, R. and Dhania, G. (2014) Tea Wastes as a Sorbent for Removal of Heavy Metals from Wastewater. *International Journal of Current Engineering and Technology*, **4**, 244-247.

[6] Buah, W., Mac Carthy, J. and Ndur, S. (2016) Conversion of Corn Cobs Waste into Activated Carbons for Adsorption of Heavy Metals from Minerals Processing Wastewater. *International Journal of Environmental Protection and Policy*, **4**, 98-103. https://doi.org/10.11648/j.ijepp.20160404.11

[7] Luo, Y. (2019) Study on the Repair of Heavy Metal Contaminated Soil. *IOP Conference Series: Earth and Environmental Science*, **300**, Article ID: 032076. https://doi.org/10.1088/1755-1315/300/3/032076

[8] Jean Claude, N., *et al.* (2022) Waste Tea Residue Adsorption Coupled with Electrocoagulation for Improvement of Copper and Nickel Ions Removal from Simulated Wastewater. *Scientific Reports*, **12**, Article No. 3519. https://doi.org/10.1038/s41598-022-07475-y

[9] Mofeed, J. (2017) Biosorption of Heavy Metals from Aqueous Industrial Effluent by Non-Living Biomass of Two Marine Green Algae *Ulva lactuca* and *Dunaliella salina* as Biosorpents. *Catrina: The International Journal of Environmental Sciences*, **16**, 43-52. https://doi.org/10.21608/cat.2017.14267

[10] Lee, A.Y.W., Lim, S.F., Chua, S.N.D., Sanaullah, K., Baini, R. and Abdullah, M.O. (2017) Adsorption Equilibrium for Heavy Metal Divalent Ions (Cu^{2+}, Zn^{2+}, and Cd^{2+}) into Zirconium-Based Ferromagnetic Sorbent. *Advances in Materials Science and Engineering*, **2017**, Article ID: 1210673. https://doi.org/10.1155/2017/1210673

[11] Sidkey, N. (2020) Biosynthesis, Characterization and Antimicrobial Activity of Iron Oxide Nanoparticles Synthesized by Fungi. *Al-Azhar Journal of Pharmaceutical Sciences*, **62**, 164-179. https://doi.org/10.21608/ajps.2020.118382

[12] Tharani, K. and Nehru, L. (2015) Synthesis and Characterization of Iron Oxide Nanoparticle by Precipitation Method. *International Journal of Advanced Research in Physical Science*, **2**, 47-50.

[13] Kheilkordi, Z., Mohammadi Ziarani, G., mohajer, F., Badiei, A. and Sillanpää, M. (2022) Recent Advances in the Application of Magnetic Bio-Polymers as Catalysts in Multicomponent Reactions. *RSC Advances*, **12**, 12672-12701. https://doi.org/10.1039/d2ra01294d

[14] Awad, M.A., Hendi, A.A., Ortashi, K.M., Alotaibi, R.A. and Sharafeldin, M.S. (2016) Characterization of Silver Nanoparticles Prepared by Wet Chemical Method and Their Antibacterial and Cytotoxicity Activities. *Tropical Journal of Pharmaceutical Research*, **15**, 679-685. https://doi.org/10.4314/tjpr.v15i4.2

[15] Kumar, V., Mohan, S., Singh, D.K., Verma, D.K., Singh, V.K. and Hasan, S.H. (2017) Photo-Mediated Optimized Synthesis of Silver Nanoparticles for the Selective Detection of Iron(III), Antibacterial and Antioxidant Activity. *Materials Science and Engineering: C*, **71**, 1004-1019. https://doi.org/10.1016/j.msec.2016.11.013

[16] Chandirika, J.U., Selvi, S.T. and Annadurai, G. (2018) Synthesis and Characterization of Silver Nanoparticle Using Melia Azedarach for Vegetable Coating and Antibacterial Activity. *Journal of Innovations in Pharmaceutical and Biological Sciences*, **5**, 38-42.

[17] Rashid, M.U., Bhuiyan, M.K.H. and Quayum, M.E. (2013) Synthesis of Silver Nano Particles (Ag-NPs) and Their Uses for Quantitative Analysis of Vitamin C Tablets. *Dhaka University Journal of Pharmaceutical Sciences*, **12**, 29-33. https://doi.org/10.3329/dujps.v12i1.16297

[18] Simon, S., Sibuyi, N.R.S., Fadaka, A.O., Meyer, M., Madiehe, A.M. and du Preez, M.G. (2021) The Antimicrobial Activity of Biogenic Silver Nanoparticles Synthesized from Extracts of Red and Green European Pear Cultivars. *Artificial Cells, Nanomedicine, and Biotechnology*, **49**, 613-624. https://doi.org/10.1080/21691401.2021.1980884

[19] Sagar, N.A., Pareek, S., Sharma, S., Yahia, E.M. and Lobo, M.G. (2018) Fruit and Vegetable Waste: Bioactive Compounds, Their Extraction, and Possible Utilization. *Comprehensive Reviews in Food Science and Food Safety*, **17**, 512-531. https://doi.org/10.1111/1541-4337.12330

[20] Rathore, G., Gupta, A. and Singh, L. (2020) An Eco-Friendly Approach for Fabrication of Silver Nanoparticles by Using Ascorbic Acid from Various Native Sources. *International Journal of Pharmaceutical Research*, **12**, 41-48.

[21] Długosz, O., Chwastowski, J. and Banach, M. (2020) Hawthorn Berries Extract for the Green Synthesis of Copper and Silver Nanoparticles. *Chemical Papers*, **74**, 239-252. https://doi.org/10.1007/s11696-019-00873-z

[22] Mohammad, D.A.E. and Taher, E.M. (2019) Antimicrobial Activity of Silver Nanoparticles Fabricated from Some Vegetable Plants. *Journal of Physics: Conference Series*, **1294**, Article ID: 062048.

[23] Chekli, L., Phuntsho, S., Roy, M. and Shon, H.K. (2013) Characterisation of Fe-Oxide Nanoparticles Coated with Humic Acid and Suwannee River Natural Organic Matter. *Science of The Total Environment*, **461**, 19-27. https://doi.org/10.1016/j.scitotenv.2013.04.083

[24] Zielińska, A., Skwarek, E., Zaleska, A., Gazda, M. and Hupka, J. (2009) Preparation of Silver Nanoparticles with Controlled Particle Size. *Procedia Chemistry*, **1**, 1560-

1566. https://doi.org/10.1016/j.proche.2009.11.004

[25] Shahat, M., Ibrahim, M., Osheba, A. and Taha, I. (2020) Preparation and Characterization of Silver Nanoparticles and Their Use for Improving the Quality of Apricot Fruits. *Al-Azhar Journal of Agricultural Research*, **45**, 33-43. https://doi.org/10.21608/ajar.2020.126625

[26] El-Khateeb, M.A. (2021) Physico-Chemical and Kinetic Evaluation of a Combined Vertical Settler/Self-Aerated Unit for Wastewater Treatment and Reuse. *CLEAN—Soil, Air, Water*, **49**, Article ID: 2100147. https://doi.org/10.1002/clen.202100147

[27] Sadon, F., Ibrahem, A.S. and Ismail, K.N. (2012) An Overview of Rice Husk Applications and Modification Techniques in Wastewater Treatment. *Journal of Purity, Utility Reaction and Environment*, **1**, 338-364.

[28] Apori, S.O., Atiah, K., Hanyabui, E. and Byalebeka, J. (2020) Moringa Oleifera Seeds as a Low-Cost Biosorbent for Removing Heavy Metals from Wastewater. *Sted Journal*, **2**, 45-52. https://doi.org/10.7251/sted2002045o

[29] Mahmoud, M.A. (2015) Thermodynamics and Kinetics Studies of Mn(II) Removal from Aqueous Solution onto Powder Corn Cobs (PCC). *Journal of Chromatography & Separation Techniques*, **6**, Article ID: 1000301. https://doi.org/10.4172/2157-7064.1000301

[30] Arunkumar, C. (2014) Use of Corn Cob as Low Cost Adsorbent for the Removal of Nickel(II) from Aqueous Solution. *International Journal of Advanced Biotechnology and Research*, **5**, 325-330.

[31] El Hotaby, W., Sherif, H.H.A., Hemdan, B.A., Khalil, W.A. and Khalil, S.K.H. (2017) Assessment of in Situ-Prepared Polyvinylpyrrolidone-Silver Nanocomposite for Antimicrobial Applications. *Acta Physica Polonica A*, **131**, 1554-1560. https://doi.org/10.12693/aphyspola.131.1554

[32] Castro, L., Rocha, F., Muñoz, J.Á., González, F. and Blázquez, M.L. (2021) Batch and Continuous Chromate and Zinc Sorption from Electroplating Effluents Using Biogenic Iron Precipitates. *Minerals*, **11**, Article No. 349. https://doi.org/10.3390/min11040349

[33] Sharma, K., Kaushik, S. and Jyoti, A. (2016) Green Synthesis of Silver Nanoparticles by Using Waste Vegetable Peel and Its Antibacterial Activities. *Journal of Pharmaceutical Sciences and Research*, **8**, 313.

[34] Shahamirifard, S.A.R., Ghaedi, M., Rahimi, M.R., Hajati, S., Montazerozohori, M. and Soylak, M. (2016) Simultaneous Extraction and Preconcentration of Cu^{2+}, Ni^{2+} and Zn^{2+} Ions Using Ag Nanoparticle-Loaded Activated Carbon: Response Surface Methodology. *Advanced Powder Technology*, **27**, 426-435. https://doi.org/10.1016/j.apt.2016.01.023

[35] Liu, Y., Liang, P. and Guo, L. (2005) Nanometer Titanium Dioxide Immobilized on Silica Gel as Sorbent for Preconcentration of Metal Ions Prior to Their Determination by Inductively Coupled Plasma Atomic Emission Spectrometry. *Talanta*, **68**, 25-30. https://doi.org/10.1016/j.talanta.2005.04.035

[36] Crini, G. (2005) Recent Developments in Polysaccharide-Based Materials Used as Adsorbents in Wastewater Treatment. *Progress in Polymer Science*, **30**, 38-70. https://doi.org/10.1016/j.progpolymsci.2004.11.002

[37] Abdelwahab, O. (2005) Use of Rice Husk for Adsorption of Direct Dyes from Aqueous Solution: A Case Study of Direct F. Scarlet. *Egyptian Journal of Aquatic Research*, **31**, 1-11.

[38] Hegazy, I., Ali, M.E.A., Zaghlool, E.H. and Elsheikh, R. (2021) Heavy Metals Adsorption from Contaminated Water Using Moringa Seeds/Olive Pomace Byproducts. *Applied Water Science*, **11**, Article No. 95. https://doi.org/10.1007/s13201-021-01421-5

[39] Lakshmi Narayan, S., Govindan, V. and Arunkumar, C. (2013) A Batch Studies on Adsorption of Nickel(II) Using Red Mud. *International Journal of Advanced Research*, **1**, 465-472.

[40] Mishra, T. and Tiwari, S.K. (2006) Studies on Sorption Properties of Zeolite Derived from Indian Fly Ash. *Journal of Hazardous Materials*, **137**, 299-303. https://doi.org/10.1016/j.jhazmat.2006.02.004

[41] Mohammadi, S.Z., Karimi, M.A., Afzali, D. and Mansouri, F. (2010) Removal of Pb(II) from Aqueous Solutions Using Activated Carbon from Sea-Buckthorn Stones by Chemical Activation. *Desalination*, **262**, 86-93. https://doi.org/10.1016/j.desal.2010.05.048

[42] Velarde, L., Nikjoo, D., Escalera, E. and Akhtar, F. (2024) Bolivian Natural Zeolite as a Low-Cost Adsorbent for the Adsorption of Cadmium: Isotherms and Kinetics. *Heliyon*, **10**, e24006. https://doi.org/10.1016/j.heliyon.2024.e24006

[43] Su, Q., He, Y., Yang, S., Wan, H., Chang, S. and Cui, X. (2021) Synthesis of NaA-Zeolite Microspheres by Conversion of Geopolymer and Their Performance of Pb(II) Removal. *Applied Clay Science*, **200**, Article ID: 105914. https://doi.org/10.1016/j.clay.2020.105914

[44] Zhu, L.K., Xi, M., Yao, Y.Y. and Lan, P. (2023) Thiol-Functionalized Activated Carbon Fibers as Efficient Adsorbents for Pb^{2+}. *Materials Chemistry and Physics*, **302**, Article ID: 127552. https://doi.org/10.1016/j.matchemphys.2023.127552

[45] Madadrang, C.J., Kim, H.Y., Gao, G., Wang, N., Zhu, J., Feng, H., *et al.* (2012) Adsorption Behavior of Edta-Graphene Oxide for Pb(II) Removal. *ACS Applied Materials & Interfaces*, **4**, 1186-1193. https://doi.org/10.1021/am201645g

[46] Alam, O., Qiao, X. and Nath, T.K. (2020) The Effect of Ca-Bearing Contents in Chitosan on Pb^{2+}, Cd^{2+} and Cu^{2+} Adsorption and Its Adsorption Mechanism. *Journal of Environmental Health Science and Engineering*, **18**, 1401-1414. https://doi.org/10.1007/s40201-020-00556-y

[47] Zhou, R., Zhang, M. and Shao, S. (2022) Optimization of Target Biochar for the Adsorption of Target Heavy Metal Ion. *Scientific Reports*, **12**, Article No. 13662. https://doi.org/10.1038/s41598-022-17901-w

[48] Aloud, S.S., Ghoneim, A., Nadim, M. and Mahdi, S. (2015) Application Efficiency of Clinoptilolite Natural Zeolite for Pb^{2+} and Cu^{2+} Removal from Wastewater. *Wulfenia*, **22**, 317-332.